Underlay of low-rate machine-type D2D links on downlink cellular links

Pratas, Nuno K.; Popovski, Petar

Published in:
2014 IEEE International Conference on Communications Workshops, ICC 2014

DOI (link to publication from Publisher):
10.1109/ICCW.2014.6881235

Publication date:
2014

Document Version
Accepted author manuscript, peer reviewed version

Underlay of Low-Rate Machine-Type D2D Links on Downlink Cellular Links

Nuno K. Pratas and Petar Popovski
Department of Electronic Systems, Aalborg University, Denmark
Email: {nup,petarp}@es.aau.dk

***Abstract*—Wireless cellular networks feature two emerging technological trends: direct Device-to-Device (D2D) communications and Machine-Type Communications (MTC). MTC devices (MTDs) pose new challenges to the cellular network, such as low transmission power and massive access that can lead to overload of the radio interface. In this paper we explore the opportunity opened by D2D links for supporting Low-rate Low-power MTDs that are connected to a nearby device, such as an on-body MTD connected to a mobile phone that acts as a relay towards the Base Station (BS). The low-rate requirement for this D2D connection allows underlay operation with Successive Interference Cancellation (SIC) during the cellular downlink transmissions. We consider different ways to use SIC and investigate the trade-off between, on one hand, the achieved rate for the downlink cellular users and, on the other hand, the outage probability for the MTC link. The results show that SIC is an important enabler of low-power underlay D2D transmission for low-rate machine-type traffic; however, it may incur a significant rate penalty for the cellular users when trying to meet the outage requirements of the MTC link.**

***Index Terms*—D2D; M2M; MTC; Underlaying; Cognitive Radio; Multiple Access Channel; SIC; OIC**

I. Introduction

Wireless cellular networks are embracing two technological trends, different from the mainstream approaches directed towards improving coverage/data rates. The first trend is the enabling of direct *Device-to-Device (D2D)* communications, by enabling direct links between the wireless devices using the same spectrum and radio interface used for cellular communications. The second trend is that of *Machine-Type Communications (MTC)* or *Machine-to-Machine (M2M)* communications [1], where a large number of low-rate low-power devices, termed *Machine-Type Devices (MTDs)*, are attached to the cellular network, enabling various applications such as large scale environment sensing, asset and health monitoring, smart grid communications, etc.

The motivation for introducing D2D communication has primarily been seen in the possibility to offload the cellular infrastructure whenever identical content needs to be served in the same localized area [2], but also in the possibility to have reliable peer-to-peer links in a licensed spectrum for sharing e.g. multimedia content. In these cases the data volumes are relatively large and therefore is worthwhile to take advantage of the high-rate D2D links. However, MTC puts forward the requirement for low-rate D2D link. For example, consider on-body sensors as MTC devices: each device requires low rate and a very low transmission power, insufficient to connect directly to the Base Station (BS). In that case, the MTC device uses a D2D link to a smart phone, which further relays the MTC traffic to the BS. In general, this type of D2D-relayed MTC can be used for other MTC applications that do not have stringent latency requirements.

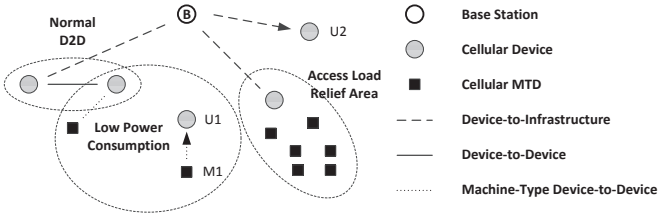

Fig. 1. Scenario illustration.

This paper explores the opportunity opened by D2D links for supporting low-rate low-power MTDs. We motivate our system model by the on-body sensing MTC devices, which can be characterized [3], [4] as having constrained battery life, for non-threatening life conditions to be delay tolerant and, due to the ubiquitous cellular coverage, to be in close proximity to a smart phone. The considered setup is shown on Fig. 1. The difference with the common usage of the D2D transmission is that here the D2D link is used for sending at a low, fixed rate and the objective is to attain a certain outage probability. The scheme in this paper treats the D2D transmission from the MTD **M1** to **U1** as an *underlay* transmission, occurring simultaneously with a downlink transmission from a BS denoted by **B** to another device **U2**. This creates a multiple access channel [5] at the receiver **U1**. The key observation is that the low rate and the low power of the MTD may allow U1 to successfully decode the downlink transmission BS-U2, cancel it, and then attempt to decode the signal from the MTD. This is reminiscent of the concept of Opportunistic Interference Cancellation (OIC), proposed for cognitive radio [6], where the primary signal can be cancelled to increase the secondary data rate. This connection is due to the fact that a D2D link acts almost as a underlay cognitive radio. The subtle difference is that here the role of the primary transmission is taken by the BS downlink transmission, but the BS is aware about the D2D link and can therefore adjust the power/rate of its transmission in order to enhance the D2D transmission, unlike the standard, non-adaptive primary in a cognitive radio model.

The main contributions of the work presented in this paper, in contrast with the works currently present in the literature [7]–[9], are the identification of the synergies between

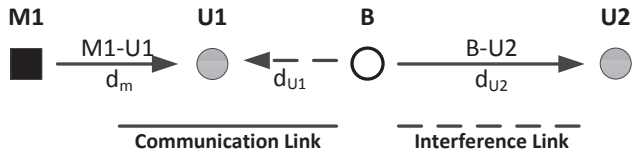

Fig. 2. Network topology.

D2D, Cognitive Radio and MTC; and investigation of the role of SIC and the trade-off between, on one hand, the achieved rate for the downlink cellular users and, on the other hand, the outage probability for the MTC link. The results show that SIC is an important enabler of low-power underlay D2D transmission for low-rate machine-type traffic; however, it may incur a significant rate penalty for the cellular users when trying to meet the outage requirements of the MTC link.

The paper is organized in the following. In Section II we described the assumed system model. In Section III we characterize four distinct underlay schemes. Followed by Section IV, where some numerical results and associated discussion presented. Finally, the paper concludes with Section V.

II. System Model

Figure 2 shows the network topology that captures the quintessential example of the transmission schemes proposed in this paper. The links are denoted by X-Y, where it is understood that X is the transmitter and Y is the receiver. All network nodes are half-duplex, i.e. a node cannot transmit and receive at the same time. The network nodes are characterized as follows:

- A Base Station (B) capable of adapting the transmission rate;
- Two *normal* devices (U1 and U2) capable of adapting the transmission rate and Multi-Packet Reception (MPR) [6] through Successive Interference Cancellation;
- One MTD, M1, which uses low transmission power and a low fixed rate R_M.

The M1 transmission is always done over the D2D link, M1-U1, at a fixed rate R_M and a requirement of maximal outage probability P_{Out}^R. On the other hand, the transmission B-U2 occurs after a process of opportunistic scheduling, in which U2 is the device within a group of N devices that supports the highest instantaneous rate. There is no interference from M1 to any cellular device due to the very low power and unfavourable propagation conditions (think of M1 as an on-body sensor), such that the rate of U2 is solely dependent on the fading for B-U2. The main ingredient of the proposed schemes is the *underlay* of link M1-U1 on B-U2, i.e. both links are simultaneously activated. We consider four operation modes, differentiated due to the way SIC is applied at U1:

- **S.1 - Perfect SIC**: This is an upper bound, in which a genie supplies U1 with the perfect version of the signal sent from B to U2, such that M1-U1 operates as if there is no interference from B;
- **S.2 - No SIC**: U1 decodes the signal from M1 by treating B's transmission as noise;
- **S.3 - Opportunistic SIC**: U1 can cancel out the interference from B and then attempt to decode the transmission from M1, whenever decoding of R_B is possible;
- **S.4 - Rate Control and SIC**: B adapts R_B to help U1 decode B's transmission and cancel it out, and therefore achieve the desired outage probability on the links M1-U1.

The scheme S.4 is classified as a network-assisted link underlay solution that, based on the collected Channel State Information (CSI) and P_{Out}^R selects the maximum allowed rate, R_B^*, of the cellular link B-U2. The rate applied on the links B-U2 are decided at the network infrastructure side; therefore the term *network-assisted*.

The downlink and the D2D transmission occur during a scheduling epoch that lasts a single time slot. All communication links are assumed to be non-Line-of-Sight and characterized by a block Rayleigh fading[1], i.e. the channel gains remain constant along the scheduling epoch. We assume that B knows the instantaneous CSI of all downlink cellular users, in order to make a proper scheduling decision. On the other hand, we assume that B knows only the CSI/fading statistics for the links towards the cellular devices that feature a D2D connection from a MTD. The reason is that, in the present scheduling epoch, those devices are not considered as candidates for downlink transmission, but rather act as receivers for the associated MTC transmission.

All the transmissions have normalized bandwidth of 1 Hz, therefore the duration of a time slot can be measured in terms of the number of symbols. The analysis here is done by considering that all communications are performed using capacity-achieving Gaussian codebooks. Furthermore, at most two simultaneous transmissions are considered over the multiple access channel, the other transmissions are modelled as noise. This is again justified by the low power applied by the other MTDs in the network. The receivers that apply interference cancellation are aware of the codebooks used by the transmitters. We note that for MTC, the assumptions of sufficient large number of symbols and Gaussian codebooks may not hold, since the MTC messages can be very short and therefore finite block length theory should be used instead in their characterization [11]. In that sense, the results shown in this paper are rather optimistic, but the approach is valid and the follow-up work can rely on the finite block length theory.

III. Transmission Schemes

In this section we characterize analytically the four schemes described in II, in a sequential manner from S.1 to S.4, starting with the preliminaries which introduce the framework over each scheme is characterized.

A. Preliminaries

As stated in II, the links M1-U1 and B-U2 occur simultaneously in a time slot. The link M1-U1 is characterized by fixed rate and power, denoted respectively as R_M and P_M. While

[1]In [10] the authors observed that with communications within the body area proximity, the short term fading follows a Rayleigh distribution.

the link B-U2 is characterized by variable rate and fixed power, hereinafter denoted respectively as R_B and P_B.

Let, in general, i denote the transmitter and j the receiver and the instantaneous received signal at node j, y_j. Therefore, the instantaneous received signal at U1, y_{U1}, and U2, y_{U2}, are given respectively by,

$$\begin{aligned} y_{U1} &= h_{M1,U1}x_{M1} + h_{B,U1}x_B + Z \\ y_{U2} &= h_{M1,U2}x_{M1} + h_{B,U2}x_B + Z \end{aligned} \tag{1}$$

where $h_{B,U1}$, $h_{B,U2}$, $h_{M1,U2}$ and $h_{M1,U1}$ denote the complex channel gains on the channel between the respective nodes. x_B and x_{M1} are respectively the signal transmitted by the B and $M1$, such that $E[|x_B|^2] = P_B$ and $E[|x_{M1}|^2] = P_M$. Z is the complex-valued Gaussian noise with variance σ^2.

Denoting $\gamma_{i,j}$ as the Signal-to-Noise Ratio (SNR), then the instantaneous achievable rate in this link is,

$$R_{i,j} = C(\gamma_{i,j}) \tag{2}$$

where $C(x)$ denotes the bandwidth normalized Shannon capacity in AWGN, given as $C(x) = \log_2(1+x)$.

Assuming that all links follow Rayleigh fading, then $|h_{i,j}|^2$ is exponential distributed with Probability Density Function (PDF), $f_{i,j}$, given by

$$f_{i,j}(x) = \frac{1}{\bar{\gamma}_{i,j}} e^{-\frac{x}{\bar{\gamma}_{i,j}}}, \text{ where } \bar{\gamma}_{i,j} = \frac{P_i L(d_{i,j})}{\sigma^2} \tag{3}$$

being $\bar{\gamma}_{i,j}$ denotes the mean $\gamma_{i,j}$, $L(d_{i,j})$ denotes the path-loss function that models the signal decay over the distance $d_{i,j}$.

To ease the notation, the SNR at the receiver of each link is denoted as follow $\gamma_M = \gamma_{M1,U1}$, $\mu_M = \gamma_{M1,U2}$, $\gamma_B = \gamma_{B,U1}$ and $\mu_B = \gamma_{B,U2}$.

The link B-U2 is established through a scheduling procedure, where the U with the higher instantaneous SNR in the scheduling epoch, from a pool of N i.i.d. UEs, is the one selected to be served. The selected UE is denoted by the label U2. The fading in this link, due to the scheduling procedure, is no longer modelled by a exponential distribution, but instead modelled by the K^{th} order statistics distribution

$$f_K(x) = Nf(x)\binom{N-1}{K-1}F(x)^{K-1}\left(1-F(x)\right)^{N-K} \tag{4}$$

where $f(x)$ and $F(x)$ are respectively the PDF and Cumulative Density Function (CDF) of the fading distribution of each individual links, K is the K^{th} selected element from the increasing ordered SNR vector and N the number of UEs. Since the scheduler selects the UE with the highest SNR, which corresponds to the case where $K = N$ and the fading distribution considered is (3), then the distribution becomes,

$$f_N(x) = Nf(x)F(x)^{N-1} = \frac{N}{\mu_B}e^{-\frac{x}{\mu_B}}\left(1-e^{-\frac{x}{\mu_B}}\right)^{N-1} \tag{5}$$

Due to $h_{M1,U2} \approx 0$, the Signal-to-Interference-plus-Noise Ratio (SINR) at U2 is simplified to SNR:

$$\frac{\mu_B}{\mu_M + 1} \xrightarrow{\mu_M << 1} \mu_B. \tag{6}$$

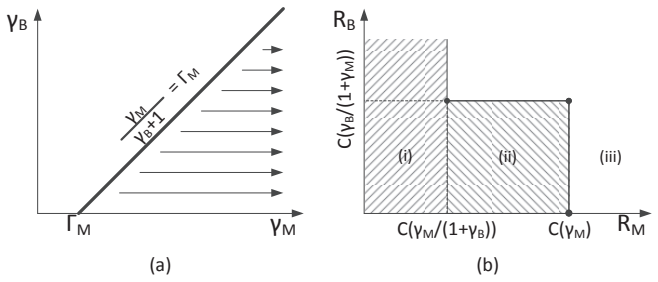

Fig. 3. (a) Integration region S.2; (b) Simplified multiple-access channel rate region at U1.

The link B-U2 has variable rate R_B, which is chosen in each time-slot so that the link is never in outage, i.e. $R_B = C(\mu_B)$. The $E[R_B]$ is then computed as follows,

$$E\left[R_B\right] = \int_0^\infty C(u) f_N\left(u\right) \mathrm{d}u \leq C(E[\mu_B]) \tag{7}$$

where the upper bound is given by the Jensen's inequality and $E\left[\mu_B\right]$ is computed as,

$$E\left[\mu_B\right] = \int_0^\infty v f_N\left(v\right) \mathrm{d}v. \tag{8}$$

When $N = 1$ then $f_1(x)$ is the exponential distribution pdf and $E\left[\mu_B\right] = \bar{\mu}_B$.

B. S.1 Perfect SIC

In the scheme S.1, there is perfect SIC: a genie provides U1 with the perfect signal replica sent by B, U1 cancels it and the decoding of the signal of M1 is free of interference. In these conditions, the link experiences outage whenever the achievable instantaneous rate goes below the target rate, i.e. $C(\gamma_M) < R_M$. From (2) the minimum SNR required to achieve R_M is then given by $\Gamma_M = 2^{R_M} - 1$. The outage probability P_{Out} for the link M1-U1, is found as:

$$P_{Out}^{S.1} = Pr\left[\gamma_M < \Gamma_M\right] = \int_0^{\Gamma_M} f_M(s)ds = 1 - e^{-\frac{\Gamma_M}{\bar{\gamma}_M}} \tag{9}$$

Therefore, to meet a given outage probability target, P_{Out}^R, the appropriate P_M and R_M needs to be selected.

C. S.2 No SIC

The probability of outage, $P_{Out}^{S.2}$ is given as,

$$P_{Out}^{S.2} = 1 - Pr\left[\frac{\gamma_M}{\gamma_B + 1} \geq \Gamma_M\right]. \tag{10}$$

Following the methodology exposed on [12], the probability $P\left[\frac{\gamma_M}{\gamma_B+1} \geq \Gamma_M\right]$ can be obtained by integrating the joint distribution, $f_{M,B}\left(s,i\right)$, in the region that meets the condition $\frac{\gamma_M}{\gamma_B+1} \geq \Gamma_M$, depicted in Figure 3(a).

As discussed in Section II, the fading channel gains for the links M1-U1 and B-U1 are independent and exponentially distributed and the respective average SNRs known, then the

joint distribution $f_{M,B}(s,i)$ is the product of the univariate marginal distributions of each link.

$$f_{M,B}(s,i) = f_M(s) f_B(i) \tag{11}$$

$$= \frac{1}{\bar{\gamma}_M \bar{\gamma}_B} e^{-\frac{s\bar{\gamma}_B + i\bar{\gamma}_M}{\bar{\gamma}_M \bar{\gamma}_B}}. \tag{12}$$

Then, $P\left[\frac{\gamma_M}{\gamma_B+1} \geq \Gamma_M\right]$ can be obtained as follows,

$$P\left[\frac{\gamma_M}{\gamma_B+1} \geq \Gamma_M\right] = \int_{\Gamma_M}^{\infty} \int_{0}^{\frac{v-\Gamma_M}{\Gamma_M}} f_{M,B}(v,u)\, du dv \tag{13}$$

$$= \frac{\bar{\gamma}_M e^{-\frac{\Gamma_M}{\bar{\gamma}_M}}}{\bar{\gamma}_M + \Gamma_M \bar{\gamma}_B}.$$

D. S.3 Opportunistic SIC

In scheme S.3, the U1 is able to perform Opportunistic Successive Interference Cancellation (OSIC) [6], where the signal coming from B can be decoded, if R_B is low enough, and subtracted from the original received signal (1) allowing the signal received from M to be decoded solely in the presence of noise. From (1) follows that if the transmissions of both B and M1 are at the receiver, then the information-theoretic setting of the Gaussian Multiple Access Channel [5] can be applied. In Figure 3(b) is depicted the simplified multiple-access channel rate region at U1. This capacity region is not convex [6], as B and M1 are not able to do time-sharing, superposition coding or any other orthogonal resource sharing scheme, while the receiver does not use joint decoding and can only decode/cancel single-user point-to-point codebooks. The shape of this capacity region is then delimited in regards to R_M as follows:

- (**i**) If $0 < R_M \leq C\left(\frac{\gamma_M}{1+\gamma_B}\right)$ - the signal from M1 can be decoded even in the presence of interference from the signal transmitted from B, therefore, there is not limit set on R_B;
- (**ii**) If $C\left(\frac{\gamma_M}{1+\gamma_B}\right) < R_{M1} \leq C(\gamma_{M1})$ - the signal from M1 can only be decoded if $R_B \leq C\left(\frac{\gamma_B}{1+\gamma_M}\right)$.
- (**iii**) If $R_{M1} > C(\gamma_M)$ - the signal from M1 cannot be decoded.

Defining $\eta_B = \frac{\gamma_B}{\gamma_M+1}$, $\eta_M = \frac{\gamma_M}{\gamma_B+1}$ and $\Gamma_B = 2^{R_B} - 1$ as the minimum SNR required to decode the signal from B with rate R_B. The probability of outage, $P_{Out}^{S.3}$, is given by

$$P_{Out}^{S.3} = 1 - P[\eta_M \geq \Gamma_M] - P[\theta] \tag{14}$$

$$\text{where } \theta = \gamma_M \geq \Gamma_M | \eta_B \geq \Gamma_B, \eta_M \leq \Gamma_M$$

The first term, $P[\eta_M \geq \Gamma_M]$, is given by (13), while the term $P[\theta]$ is derived as follows. Consider the following equations,

$$\frac{\gamma_M}{\gamma_B+1} = \Gamma_M \Longleftrightarrow \gamma_M = \Gamma_M(\gamma_B+1) \tag{15}$$

$$\frac{\gamma_B}{\gamma_M+1} = \Gamma_B \Longleftrightarrow \gamma_B = \Gamma_B(\gamma_M+1)$$

which denote respectively two lines which intersect at the coordinate,

$$\left(\gamma_M^{Int}, \gamma_B^{Int}\right) = \left(\frac{\Gamma_M(\Gamma_B+1)}{1-\Gamma_M\cdot\Gamma_B}, \frac{\Gamma_B(\Gamma_M+1)}{1-\Gamma_M\cdot\Gamma_B}\right). \tag{16}$$

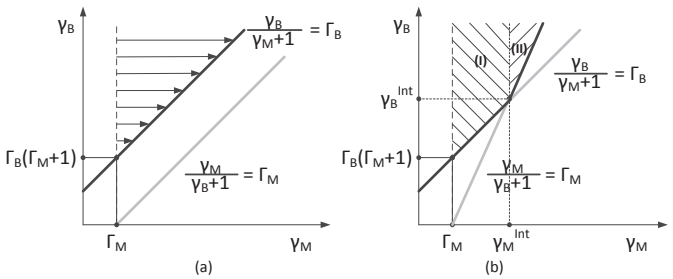

Fig. 4. (a) Integration region when $\Gamma_M \cdot \Gamma_B > 1$ (b) Integration region when $\Gamma_M \cdot \Gamma_B < 1$.

The intersection point occurs in third quadrant of the γ_M γ_B plane when $\Gamma_M\Gamma_B > 1$, while when $\Gamma_M\Gamma_B < 1$ it occurs in the first quadrant. The point of intersection is important since it will decide which of the integration regions depicted in Figure 4 should be considered to obtain the correct outage probability. When $\Gamma_M\Gamma_B > 1$, for which the integration region is shown in Figure 4(a), the term $P[\theta]$ of (14) is given as follows,

$$P_{\Gamma_M\Gamma_B>1}[\theta] = \int_{\Gamma_B(\Gamma_M+1)}^{\infty} \int_{\Gamma_M}^{\frac{u-\Gamma_B}{\Gamma_B}} f_{M,B}(v,u)\, dv du \tag{17}$$

$$= \bar{\gamma}_B \frac{e^{-\frac{\Gamma_B\bar{\gamma}_M(\Gamma_M+1)-\Gamma_M}{\bar{\gamma}_B\bar{\gamma}_M}}}{\bar{\gamma}_B + \Gamma_B\bar{\gamma}_M}$$

When $\Gamma_M\Gamma_B < 1$, as depicted in Figure 4(b), there are two integration regions of interest. The second term of (14) is then given by (18).

The success probability given Γ_B, $f_S(\Gamma_B)$, is defined as,

$$f_S(\Gamma_B) = P[\eta_M \geq \Gamma_M] + \begin{cases} P_{\Gamma_M\Gamma_B>1}[\theta] & \Gamma_M\Gamma_B > 1 \\ P_{\Gamma_M\Gamma_B<1}[\theta] & \Gamma_M\Gamma_B < 1 \end{cases} \tag{19}$$

Similarly to S.2 and S.3 R_B is selected such that the link B-U2 is never in outage and so Γ_B becomes dependent on the instantaneous channel conditions of the link B-U2, i.e. $\Gamma_B = \mu_B$. Therefore, to compute the $P_{Out}^{S.3}$ it is necessary to average (19) over the density of the random variable μ_B. Defining the identity $\Theta(g(u),a) = \int_0^a g(u) f_N(u)\, du$, then $P_{Out}^{S.3}$ is given as follows,

$$P_{Out}^{S.3} = 1 - \Theta(f_S(u), \infty). \tag{20}$$

which is evaluated through numerical integration methods.

E. S.4 Rate Control and SIC

In the scheme S.4, similarly to S.3 the U1 is able to decode the signal coming from B and then subtract it from the original received signal, with the main difference that a maximum allowed R_B^* is selected in each scheduling epoch such that the outage probability target in the M1-U1 link is met, i.e. $P_{Out}^R \geq P_{Out}^{S.4}$.

The mean rate R_B is now dependent on the upper ceiling given by R_B^*. Defining $\Gamma_B^* = 2^{R_B^*} - 1$ and assuming the upper bound given in (7) holds, then $E[R_B | R_B \leq R_B^*]$ is upper bounded as follows,

$$E[R_B | R_B \leq R_B^*] \leq C(E[\mu_B | \mu_B \leq \Gamma_B^*]), \tag{21}$$

$$P_{\Gamma_M\Gamma_B<1}[\theta] = \int_{\Gamma_M}^{\frac{\Gamma_M(\Gamma_B+1)}{1-\Gamma_M\Gamma_B}} \int_{\Gamma_B(u+1)}^{\infty} f_{\gamma_M,\gamma_B}(v,u)\,dvdu + \int_{\frac{\Gamma_B(\Gamma_M+1)}{1-\Gamma_M\Gamma_B}}^{\infty} \int_{\frac{\Gamma_M(\Gamma_B+1)}{1-\Gamma_M\Gamma_B}}^{\Gamma_M(v+1)} f_{\gamma_M,\gamma_B}(v,u)\,dudv \quad (18)$$

$$= \phi - \frac{\bar{\gamma}_B e^{-\frac{\Gamma_B}{\bar{\gamma}_B}}\left(\phi - e^{-\frac{\Gamma_M(\Gamma_B\bar{\gamma}_M+\bar{\gamma}_B)}{\bar{\gamma}_B\bar{\gamma}_M}}\right)}{(\bar{\gamma}_B+\Gamma_B\bar{\gamma}_M)} - \frac{\bar{\gamma}_M\phi e^{-\frac{\Gamma_M}{\bar{\gamma}_M}}}{(\bar{\gamma}_M+\Gamma_M\bar{\gamma}_B)} \text{where } \phi = e^{\frac{\Gamma_B(\Gamma_M+1)}{\bar{\gamma}_B(\Gamma_B\Gamma_M-1)}} e^{\frac{\Gamma_M(\Gamma_B+1)}{\bar{\gamma}_M(\Gamma_B\Gamma_M-1)}}.$$

Algorithm 1: Maximum allowed R_B^*.

Input Parameters: μ_B, $\bar{\gamma}_B$, $\bar{\gamma}_M$, Γ_M, ϵ, P_{Out}^R

Ouput Parameter: R_B^*

Algorithm:

`/* Find maximum allowed` $\tilde{R}_B$ `*/`

$max\ \tilde{R}_B$ such that $\left|P_{Out}^{S.4}\left(\tilde{R}_B\right) - P_{Out}^{Target}\right| < \epsilon$

`/* Check if link B-U2 can support it */`

$$R_B^* = \begin{cases} C(\mu_B) & \tilde{R}_B \geq C(\mu_B) \\ R_B^* & \tilde{R}_B < C(\mu_B) \end{cases}$$

where $E[\mu_B|\mu_B \leq \Gamma_B^*]$ is given by,

$$E[\mu_B|\mu_B \leq \Gamma_B^*] = \Theta(u,\Gamma_B^*) + (1-\Theta(1,\Gamma_B^*))\,\Gamma_B^*. \quad (22)$$

We note that this approximation matches closely the simulation results. For N = 1, $E[\mu_B|\mu_B \leq \Gamma_B^*] = \bar{\mu}_B\left(1 - e^{-\frac{\Gamma_B^*}{\bar{\mu}_B}}\right)$.

The outage probability, $P_{Out}^{S.4}(R_B^*)$, is defined as,

$$P_{Out}^{S.4}(R_B^*) = \quad (23)$$
$$1 - [\Theta(f_S(v),\Gamma_B^*) + (1-\Theta(1,\Gamma_B^*))\,f_S(\Gamma_B^*)],$$

and evaluated through numerical integration methods.

The core of the procedure that selects the maximum R_B^* that meets P_{Out}^R within an error tolerance ϵ, listed on Algorithm 1, is based on the computation of (23). This procedure requires the knowledge of the fading distributions in each of the links, as well as the channel statistics in the M1-U1 and B-U1 links and the channel realization in the link B-U2.

The maximization problem stated in the algorithm can be solved using root finding methods such as Brent's method.

IV. Numerical Results and Discussion

In this section we present two sets of numerical results corresponding respectively to the analysis of the schemes S.1 to S.4 and of the scheme S.4 with various R_M. These numerical results were obtained by evaluating the corresponding analytical expressions derived in the previous section as well as through stochastic simulations. Table I lists the relevant system parameters, where L_M and $L(d_x)$ denote respectively the pathloss in the M1-U1 link and any other links.

A. Performance Comparison

In Figures 5 and 6 the $E[R_B]$ and P_{Out} are plotted when $d_{U2} = \{20\}$ and $d_{U2} = \{80\}$ which correspond to near/distant position of the cluster of cellular users from which U2 is selected. The plots show a drop in the value $E[R_B]$ in scheme S.4, when $d_{U1} < 120$. The distance region where this drop occurs, corresponds to the case where the rate control mechanism is enacted so to ensure that the outage target is met. In the P_{Out} plots, particularly the one for S.3, it can be seen that there is a spike on the outage that corresponds to the same region where the R_B control mechanism is active. Another interpretation is that this region corresponds to the case where OIC occurs, since the observed outage probability is lower than the one in S.2, but it loses its effectiveness as the distance between U1 and B increases. Therefore the only way to maintain the outage probability is to control R_B. When comparing Figures 5 and 6, it can be seen that the drop in $E[R_B]$ is less accentuated in the later case. This is due to the U2 being at larger distance from B and therefore the achievable rates will be much smaller. The cellular transmissions directed to distant (cell-edge located) cellular devices that due to the path loss attenuation lead to lower achievable rates, as shown in Figure 6, are seen as good candidates to be underlayed by Machine-Type D2D links, since the impact of the rate control is lower compared to the cellular users closer to the base station. The traditional power control algorithms, widely present in the relevant literature, would apply to the scheme S.2, which as shown will lead to much lower cellular rates than the SIC based solutions here considered. Finally, it should be emphasized that the proposed rate control mechanism always selects the R_B that meets the target requirement for outage

Parameter	Value	Parameter	Value
$L(d_x)$	[13, C1,NLOS,$f_c = 2.1GHz$]	N	20
L_M	$-60[dB]$ [14]	P_{Out}^R	0.1
σ^2	$-97.5[dBm]$ [15]	ϵ	0.001
P_B	$46[dBm]$	P_M	$0[dBm]$
d_{U2}	$20, 80[m]$	d_M	$1[m]$

TABLE I
Simulation scenario settings.

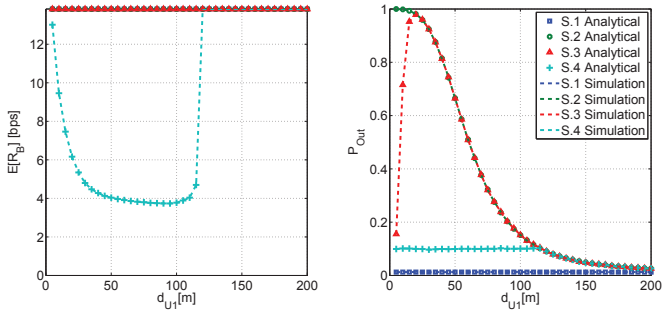

Fig. 5. $E[R_B]$ and P_{Out} when $d_{U2} = 20$ and $R_M = 0.1$.

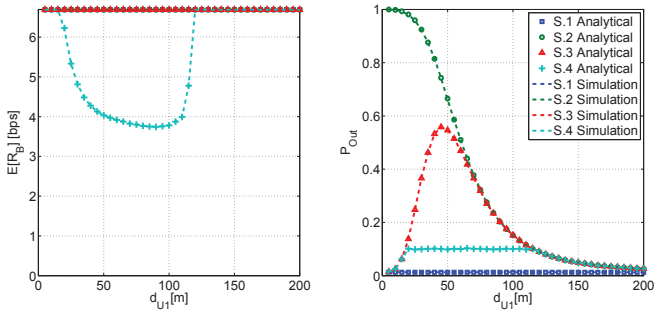

Fig. 6. $E[R_B]$ and P_{Out} when $d_{U2} = 80$ and $R_M = 0.1$.

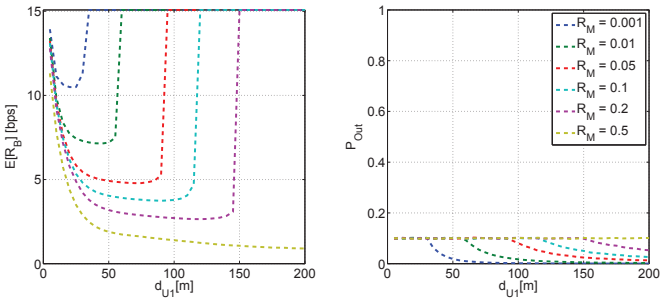

Fig. 7. $E[R_B]$ and P_{Out} when $d_{U2} = 20$.

probability, by using the knowledge of the instantaneous realization of the channel between B and U2 as well as the knowledge of the link fading distribution.

B. Performance with R_M

Figure 7 depicts $E[R_B]$ and P_{Out} when $d_{U2} = 20$ for various values of R_M. The key observation is that the lower is the R_M, then the smaller is the region where the rate control mechanism is enacted. From these results, it is seen that when the MTC link occurs near B, its underlay on the cellular downlink occurs with some downlink rate penalty, although at a larger distance this penalty no longer occurs, since the SIC no longer takes place. Further, to enable the successful deployment of Machine-Type D2D connectivity closer to the cell, these results motivate the introduction of SIC capable cellular devices.

V. Conclusion

We proposed a network assisted device-to-device solution that enables the cooperation between Machine-Type cellular devices and normal cellular devices, while reducing the outage of the machine-type communications and maximizing the combined cellular system rate. The model captures the main performance objectives: outage probability for a given low fixed rate for the Machine-Type communication versus rate maximization for the cellular broadband traffic. System rate maximization is accomplished by the underlay of device-to-device link on the cellular link in the downlink direction. Successive Interference Cancellation (SIC) is an important enabler of underlay D2D communication and is particularly suitable in conjunction with low-rate MTC signal transmission over the D2D link. The results from this paper show that low power, fixed rate Machine-Type devices can share the air interface with normal cellular devices, but there can be a rate penalty for the cellular users. This occurs even when it is assumed that there is no interference from the MTC transmissions to the downlink signals received by the other cellular users and is a result of the rate control for the cellular users in order to meet outage requirements for the MTC users. In our future work we will investigate the system-level performance of these schemes by using the tools of stochastic geometry and considering random deployment of the cellular and MTC devices.

Acknowledgment

We would like to acknowledge our colleague Nurul H. Mahmood for the discussions on SIC modelling. The research presented in this paper was partly supported by the Danish Council for Independent Research (Det Frie Forskningsråd) within the Sapere Aude Research Leader program, Grant No. 11-105159 "Dependable Wireless Bits for Machine-to-Machine (M2M) Communications" and performed partly in the framework of the FP7 project ICT-317669 METIS. The authors would like to acknowledge the contributions of their colleagues in METIS, although the views expressed are those of the authors and do not necessarily represent the project.

References

[1] D. Boswarthick, O. Elloumi, and O. Hersent, *M2M Communications: A Systems Approach*. Wiley, 2012.
[2] M. Ji, G. Caire, and A. F. Molisch, "Wireless Device-to-Device Caching Networks: Basic Principles and System Performance," *ArXiv e-prints*, May 2013.
[3] F. Viani, F. Robol, A. Polo, P. Rocca, G. Oliveri, and A. Massa, "Wireless architectures for heterogeneous sensing in smart home applications: Concepts and real implementation," *Proceedings of the IEEE*, vol. 101, no. 11, pp. 2381–2396, 2013.
[4] I. Korhonen, J. Parkka, and M. Van Gils, "Health monitoring in the home of the future," *Engineering in Medicine and Biology Magazine, IEEE*, vol. 22, no. 3, pp. 66–73, 2003.
[5] A. Gamal and Y. Kim, *Network Information Theory*. Cambridge University Press, 2011.
[6] R. Di Taranto and P. Popovski, "Outage performance in cognitive radio systems with opportunistic interference cancelation," *Wireless Communications, IEEE Transactions on*, vol. 10, no. 4, pp. 1280–1288, 2011.
[7] A. Asadi, Q. Wang, and V. Mancuso, "A survey on device-to-device communication in cellular networks," *CoRR*, vol. abs/1310.0720, 2013.
[8] G. Fodor, E. Dahlman, G. Mildh, S. Parkvall, N. Reider, G. Miklos, and Z. Turanyi, "Design aspects of network assisted device-to-device communications," *Communications Magazine, IEEE*, vol. 50, no. 3, pp. 170–177, 2012.
[9] X. Lin, J. G. Andrews, A. Ghosh, and R. Ratasuk, "An overview on 3gpp device-to-device proximity services," *CoRR*, vol. abs/1310.0116, 2013.
[10] S. Heaney, W. Scanlon, E. Garcia-Palacios, and S. Cotton, "Fading characterization for context aware body area networks (caban) in interactive smart environments," in *Antennas and Propagation Conference (LAPC), 2010 Loughborough*, pp. 501–504, 2010.
[11] Y. Polyanskiy, H. Poor, and S. Verdu, "Channel coding rate in the finite blocklength regime," *Information Theory, IEEE Transactions on*, vol. 56, no. 5, pp. 2307–2359, 2010.
[12] N. H. Mahmood, L. G. U. Garcia, P. Popovski, and P. E. Mogensen, "On the performance of successive interference cancellation in 5g small cell networks," *WCNC 2014*, 2014.
[13] D1.1.2, "Part i channel models," tech. rep., WINNER II, 2007.
[14] K. Yazdandoost] and K. Sayrafian-Pour, "Ieee p802.15-08-0780-09-0006," tech. rep., IEEE P802.15, 2009.
[15] A. T. Harri Holma, ed., *LTE for UMTS: Evolution to LTE-Advanced, 2nd Edition*. Wiley, 2011.